BAMS Article

Pronounced Impact of Salinity on Rapidly Intensifying Tropical Cyclones

Karthik Balaguru, Gregory R. Foltz, L. Ruby Leung, John Kaplan, Wenwei Xu, Nicolas Reul, and Bertrand Chapron

ABSTRACT: Tropical cyclone (TC) rapid intensification (RI) is difficult to predict and poses a formidable threat to coastal populations. A warm upper ocean is well known to favor RI, but the role of ocean salinity is less clear. This study shows a strong inverse relationship between salinity and TC RI in the eastern Caribbean and western tropical Atlantic due to near-surface freshening from the Amazon–Orinoco River system. In this region, rapidly intensifying TCs induce a much stronger surface enthalpy flux compared to more weakly intensifying storms, in part due to a reduction in SST cooling caused by salinity stratification. This reduction has a noticeable positive impact on TCs undergoing RI, but the impact of salinity on more weakly intensifying storms is insignificant. These statistical results are confirmed through experiments with an ocean mixed layer model, which show that the salinity-induced reduction in SST cold wakes increases significantly as the storm's intensification rate increases. Currently, operational statistical–dynamical RI models do not use salinity as a predictor. Through experiments with a statistical RI prediction scheme, it is found that the inclusion of surface salinity significantly improves the RI detection skill, offering promise for improved operational RI prediction. Satellite surface salinity may be valuable for this purpose, given its global coverage and availability in near–real time.

https://doi.org/10.1175/BAMS-D-19-0303.1
Corresponding author: Gregory R. Foltz, gregory.foltz@noaa.gov
Supplemental material: https://doi.org/10.1175/BAMS-D-19-0303.2
In final form 17 March 2020

AFFILIATIONS: Balaguru, Leung, and Xu—Pacific Northwest National Laboratory, Richland, Washington; **Foltz and Kaplan**—NOAA/Atlantic Oceanographic and Meteorological Laboratory, Miami, Florida; **Reul and Chapron**—Laboratoire d'Océanographie Physique et Spatiale, Ifremer, Brest, France

Rapid intensification (RI) of tropical cyclones (TCs), defined as the 95th percentile of 24-h over-water intensity changes, or an increase in intensity of at least 30 kt (1 kt ≈0.51 m s^{-1}) in a 24-h period, is extremely difficult to predict. The challenge is at the forefront of operational TC forecasting (Gall et al. 2013). Considering that all category 4 and 5 TCs in the Atlantic undergo RI during their lifetimes (Kaplan and DeMaria 2003), the significance of RI is disproportionately high relative to the low chance of occurrence (Lee et al. 2016). The hyperactive 2017 Atlantic TC season was extremely destructive, with several intense TCs making devastating landfalls after undergoing RI (Rahmstorf 2017; Balaguru et al. 2018; Klotzbach et al. 2018). In 2018, TCs Florence and Michael underwent unanticipated explosive RI in the eastern Atlantic and in the Gulf of Mexico, before impacting the Carolinas and the Florida panhandle, respectively (Avila 2019). More recently, in August 2019 TC Dorian underwent RI to the north of the Caribbean Sea before scything through the Bahamas. With RI of TCs projected to rise in coastal regions just before landfall under climate change (Emanuel 2017), there is a critical need to improve our understanding of the phenomenon.

TCs intensify by extracting heat energy from the ocean. Sea surface temperature (SST) under the core of the storm, and processes that govern its evolution, therefore play a critical role in TC intensification (Emanuel 1999; Cione and Uhlhorn 2003). When over the ocean, a TC's intense winds induce vertical mixing and sea surface cooling that acts as a negative feedback on the storm's intensity, causing upper-ocean density stratification to affect the storm's intensification (Price 1981; Bender and Ginis 2000; Cione and Uhlhorn 2003). While some studies suggest that processes typically favoring TC intensification are also responsible for RI (Kowch and Emanuel 2015), others indicate that we need to improve our understanding of mechanisms governing RI (Rozoff and Kossin 2011).

For operational forecasting of RI, some of the best performing models are statistical (Kaplan et al. 2015). In these models, environmental parameters that influence RI are combined using statistical techniques such as linear discriminant analysis, logistic regression, or Bayesian methods in order to predict the chance of RI occurrence (Kaplan et al. 2010; Rozoff and Kossin 2011; Kaplan et al. 2015). Typically, SST and tropical cyclone heat potential (TCHP), metrics for the warmth of the ocean surface and the depth of the warm water reservoir (Shay et al. 2000), respectively, are used to represent the ocean in these models (Kaplan et al. 2010, 2015). Though SST and TCHP include effects of upper-ocean thermal structure, they do not incorporate salinity impacts on ocean stratification (Balaguru et al. 2015). This leads to the following question: Does salinity play a role in RI? In the western tropical Atlantic, near-surface ocean stratification is substantially enhanced by the freshwater lens of the Amazon–Orinoco River system, which acts to inhibit TC-induced oceanic mixing and SST cooling (Balaguru et al. 2012; Grodsky et al. 2012). While several previous studies have shown varying degrees of salinity impact on TC intensification (Balaguru et al. 2012; Grodsky et al. 2012; Reul et al. 2014; Newinger and Toumi 2015; Androulidakis et al. 2016; Yan et al. 2017; Rudzin et al. 2019; Hlywiak and Nolan 2019), its specific role in RI has not been evaluated.

Irma, the strongest TC from the 2017 Atlantic TC season based on maximum sustained winds, reached a peak intensity of 155 kt and maintained category 5 strength longer than any other TC in the world (Rahmstorf 2017; Klotzbach et al. 2018). Between 4 and 6 September,

Irma underwent a phase of RI to the east of the Caribbean Islands before making destructive landfalls in the Leeward Islands of the West Indies, Cuba, and the Florida Keys. The upper-ocean state just before TC Irma formed on 30 August suggests that as the storm moved west of 50°W, it encountered an increasingly favorable ocean (Figs. 1a,b). SSTs exceeded 28°C and TCHP was higher than 50 kJ cm^{-2} in much of the western Atlantic. The largest values of SST and TCHP, exceeding 29°C and 100 kJ cm^{-2}, respectively, were found in the northwestern Caribbean Sea and near the entrance to the Gulf of Mexico. The spatial variability of sea surface salinity (SSS), on the other hand, is dominated by the freshwater plume of the Amazon–Orinoco River system, stretching approximately from 50° to 70°W and from the South American coast to 25°N (Fig. 1c). Irma appears to have traversed the plume when it underwent RI. The storm commenced strengthening just to the west of 50°W and subsequently entered a phase of RI, centered around 55°W, where it increased in intensity from category 3 to category 5 (Fig. 1c). During this period, SST and TCHP increased by about 1°C and 30 kJ cm^{-2}, respectively (Figs. 1d,e). However, the TC also encountered nearly a 2 psu drop in salinity between 50° and 55°W when it underwent RI (Fig. 1f).

Matthew, the most powerful TC from the 2016 season (Stewart 2017), also appears to have undergone RI over low-salinity plume waters to the north of Venezuela in the Caribbean Sea [see Figs. ES1a,b in the online supplemental material (https://doi.org/10.1175/BAMS-D-19-0303.2)]. A brief examination of along-track conditions for Gonzalo (2014), a category 4 TC that caused widespread destruction in the Leeward Islands and Bermuda, indicates that it also underwent

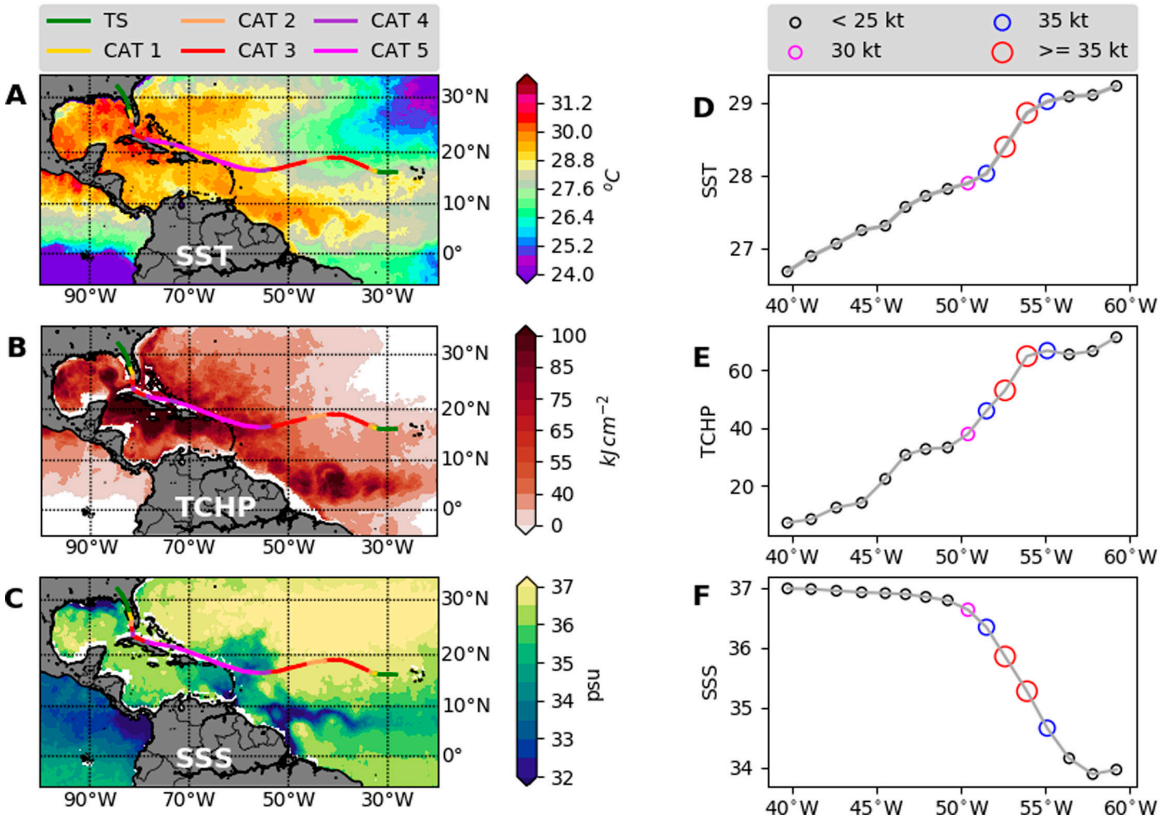

Fig. 1. (a) SST (°C) and (b) TCHP (kJ cm^{-2}) on 29 Aug, and (c) SSS (psu) averaged between 19 and 27 Aug, with the track of TC Irma (2017), color coded by its intensity, overlaid. The legend shown above (a) corresponds to the strength of Irma based on the Saffir–Simpson hurricane wind scale. SST is from the satellite-based REMSS product, TCHP is based on HYCOM, and SSS is obtained from SMOS satellite. Along-track (d) SST (°C), (e) TCHP (kJ cm^{-2}), and (f) SSS (psu) for TC Irma. The circles in (d)–(f) represent the 24-h intensity change at various 6-h locations, with black denoting non-RI and color denoting RI. The legend shown above (d) corresponds to the magnitude of 24-h intensity change experienced by Irma.

RI while over the freshwater plume near Puerto Rico (Figs. ES1c,d; Domingues et al. 2015). Similarly, Igor, an intense category 4 TC from the 2010 season likely intensified rapidly over the northern tip of the Amazon River plume (Reul et al. 2014). Hence, this preliminary examination of a few TCs raises the following question: Can the influence of the ocean on RI be attributed mostly to the upper-ocean thermal structure, or does salinity also play an important role? In this study, using a combination of observations and numerical model simulations, we explore the potential role of salinity in RI.

Methods

Data. Atlantic TC best track data (HURDAT2) for the period 2002–18, obtained from the National Hurricane Center (www.nhc.noaa.gov; Landsea and Franklin 2013), are used to identify storm locations and to derive TC intensification rates. We use daily optimally interpolated SST from Remote Sensing Systems (www.remss.com) for the period 2002–18 at a 9 km spatial resolution to estimate prestorm SST (defined as SST three days before the storm's arrival) and TC-induced cold wakes or SST cooling (estimated as the difference between SST on the day of the TC and the prestorm SST) along the storms' tracks. This product combines data from all available infrared and microwave satellites. Daily objectively analyzed air–sea fluxes (OAFlux; Yu et al. 2008), obtained from http://oaflux.whoi.edu for the period 2002–18, are used to estimate the enthalpy flux at the air–sea interface under TCs. Enthalpy flux is computed as the sum of latent and sensible heat fluxes on the day of the TC. Although the product is available at a spatial resolution of 1°, it has been used to understand air–sea heat fluxes under TCs previously (Balaguru et al. 2012). All data are obtained beginning in 2002, when the satellite-based Remote Sensing Systems SST data are made available.

Along-track TCHP is calculated using vertical ocean temperature profiles from HYCOM Global Ocean Forecast System version 3.1 reanalysis (Chassignet et al. 2007). In addition to TCHP, prestorm ocean temperature and salinity profiles are used to calculate ocean density, temperature, and salinity stratification along TC tracks. HYCOM reanalysis is available at 3-hourly frequency and at an eddy-resolving 8 km spatial resolution from www.hycom.org. The vertical resolution in the upper 100 m varies from 2 to 10 m, with higher resolution close to the surface. We extract data at daily frequency for our calculations. As for prestorm SST, various parameters are obtained from HYCOM three days before the storm's arrival. To validate our main results based on HYCOM, we use vertical ocean temperature and salinity profiles from version 3.4.2 of the Simple Ocean Data Assimilation (SODA) reanalysis (Carton et al. 2018), available at a 0.5° spatial resolution and as 5-day means from www.soda.umd.edu. In the upper 100 m, the vertical resolution is approximately 10 m. TCHP, ocean stratification, and SSS are obtained from SODA over the 5-day period prior to the storm's arrival. The HYCOM and SODA 3.4.2 reanalyses are available for the periods 1994–2015 and 1980–2017, respectively. In this study, data are used beginning in 2004 since the availability of Argo floats makes estimates of the ocean subsurface more reliable over this period (Baker et al. 2019). Nine-day mean SSS measurements from the Soil Moisture and Ocean Salinity (SMOS) satellite (Boutin et al. 2017), available from www.catds.fr at a resolution of 0.25° and for the period 2010–17, are used to estimate prestorm ocean salinity along TC tracks. These data are used to provide an independent validation of HYCOM, and to show the potential value of satellite SSS for prediction. Prestorm SSS is calculated as the SSS averaged over the 9-day period prior to the storm. Note that the time periods for various datasets differ slightly in order to maximize the data used for different analyses.

We explore the impact of salinity on vertical mixing and thus TC-induced SST cooling by using the Price–Weller–Pinkel (PWP) one-dimensional ocean mixed layer model (Price et al. 1986). Model input data are composed of 20 Argo float temperature and salinity profiles within the region 10°–20°N, 70°–50°W during August–October 2016–18 ("PWP model experiments" section).

Developmental data for various predictors of the Statistical Hurricane Intensity Prediction Scheme Rapid Intensification Index (SHIPS-RII) were obtained from http://rammb.cira.colostate.edu/research/tropical_cyclones/ships/developmental_data.asp. These data describe the large-scale TC environment and are derived from gridded operational global analyses (DeMaria et al. 2005). We combine these developmental data and salinity with a statistical model ("Significance of salinity for RI prediction" section) to understand the value of salinity for predicting RI.

Calculations. TCHP is calculated as the integral of the temperature from the surface to the depth of the 26°C isotherm:

$$\mathrm{TCHP} = \rho C_p \int_0^{Z26} [T(z) - 26]\, dz, \tag{1}$$

where ρ is the seawater density, C_p is the seawater specific heat capacity, $T(z)$ is the seawater temperature as a function of water depth, and Z26 is the depth of the 26°C isotherm (Shay et al. 2000). Temperature, salinity, and density stratification are defined as the difference between the respective variable at a depth of 100 m and the surface value. The above calculations are performed using data from HYCOM and SODA. Track locations contaminated with land effects are excluded from our analysis. Intensity change over a period is calculated as the difference between the intensity at the end of that period and the initial intensity.

PWP model experiments. The forcings for the PWP model are the surface heat and moisture fluxes, which here are set to zero throughout the model integrations, and wind stress (Balaguru et al. 2015). The model's mixed layer entrains successively deeper water until the bulk Richardson number exceeds 0.65. Vertical mixing is then performed beneath the mixed layer until the gradient Richardson number between each level is greater than 0.25.

The model was initialized with vertical profiles of temperature and salinity from Argo floats in the western tropical Atlantic and eastern Caribbean Sea (10°–20°N, 50°–70°W) during August–October 2016–18. Based on a decorrelation length scale for salinity in the western tropical Atlantic of about 3° (Sena Martins et al. 2015), we chose 20 profiles to approximately represent the range of salinity conditions found in this region. Most of the 20 included profiles exhibit strong salinity stratification in the upper 50 m. Two sets of experiments were conducted, each initialized with one of the 20 Argo profiles. The first set of experiments was initialized with observed temperature and salinity, the second with observed temperature and vertical mean salinity at every depth. In addition, we varied the model's wind forcing to test the impact of intensification rate on salinity-induced SST cooling as described below.

The model was forced with winds from TCs with idealized surface circulations: The surface wind field was assumed to be axisymmetric, with the wind speed a function only of the storm's maximum wind speed, radius of maximum winds (r_m), and distance from the storm's center (DeMaria 1987) as follows:

$$V(r) = V_m \left(\frac{r}{r_m}\right) \exp\left[\frac{1}{b}\left(1 - \frac{r}{r_m}\right)^b\right]. \tag{2}$$

Here, $V(r)$ is the tangential wind as a function of distance r from the storm center and r_m is the radius of maximum tangential winds (V_m). We used a constant value of 0.9 for b in this equation, giving a radius of 23 kt (12 m s^{-1}) winds of ~200 km. For all simulations, an r_m of 50 km was used. With these parameters and the storm's translation speed of 5 m s^{-1} (9.7 kt), the wind speed was calculated as a function of time along a north–south axis running through the storm's center while accounting for the translation velocity. As the storm moves northward, the wind speed therefore increases from 25 kt to $w_{\mathrm{tot}} = \sqrt{w^2 + 9.7^2}$ as the northern

eyewall passes, where w is the storm's maximum rotational wind speed in knots and w_{tot} is the magnitude of the vector sum of the maximum rotational velocity and translation velocity. The wind speed then goes to zero in the eye and back up to w_{tot} in the southern eyewall, here referred to as the second r_m.

We performed a control simulation in which the maximum wind was set to 60 kt, the approximate mean intensity of all TCs in the western tropical Atlantic (10°–30°N, 60°–100°W). We then conducted an experiment in which the wind profile was decreased linearly along the track (starting with no change at $t = 0$) so that the maximum wind speed at the second r_m, located 250 km, or about 14 h, from the start of the integration, was 40 kt. A similar experiment was conducted so that the maximum wind speed at the second r_m was 20 kt. The percentage reduction in wind speed was held constant from the second r_m until the end of the integration time period, which was 24 h. Similar experiments were performed in which the maximum wind was increased to either 80 or 100 kt. In total, 200 model runs were performed (20 different initial profiles, each with observed and vertical mean salinity, and for five different TC wind scenarios).

Significance of salinity for RI prediction. To quantify the relevance of salinity for RI, we perform binary classification using the statistical scheme of logistic regression. A statistical binary classification model combines several parameters to predict a binary-dependent variable, which in this case is the occurrence of RI. The SHIPS-RII predictors used are previous 12-h intensity change or persistence (PER), 850–200 hPa vertical wind shear within a 500 km radius after vortex removal (SHRD), 200 hPa divergence within a 1,000 km radius (D200), percent areas with total precipitable water <45 mm within a 500 km radius and ±45° of the upshear SHIPS wind direction (TPW), second principal component of GOES-IR imagery within a 440 km radius (PC2), standard deviation of GOES-IR brightness temperature within a 50–200 km radius (SDBT), potential intensity (POT), TCHP, inner-core dry-air predictor (ICDA), and initial intensity (VMX0) (Kaplan et al. 2015). These 10 predictors are available for each 6-hourly TC track location. Among them, SHRD, D200, POT, TCHP, and ICDA are averaged over the 24-h forecast period (Kaplan et al. 2015). Two sets of predictions are performed: one using only these 10 predictors, the other including SSS as an additional predictor.

First we divide the dataset, which contains the various SHIPS-RII predictors and SSS estimated for the corresponding 6-hourly locations, into two subsets: one for cases in which TCs underwent RI and another for cases in which TCs did not undergo RI. Next we choose fractions of the data from the two subsets (specified later in this section) and combine them into the training set. The remaining data from the two subsets are then combined into a test set. We train the classification model on the training set and use the trained model to make predictions for the test set.

Based on the predictions for the test set, we estimate the skill of the model using four different metrics: probability of detection (POD), false alarm ratio (FAR), area under the receiver operating characteristic (AUROC), and the Brier score (BS). A true positive (TP) is defined as a situation when the model correctly predicts the occurrence of RI. A true negative (TN) is defined as a situation when the model correctly predicts the nonoccurrence of RI. A false positive (FP) is defined as an event where the model incorrectly predicts that an RI will occur, while a false negative (FN) is defined as an event where the model incorrectly predicts that an RI will not occur. With these definitions, the various metrics used to assess the model (www.cawcr.gov.au/projects/verification/) are calculated as follows. The POD indicates the number of correctly predicted RI events out of the total number of actual RI events [TP/(TP + FN)]. The FAR represents the number of times RI was wrongly predicted to occur out of the total number of times the model predicted RI [FP/(TP + FP)]. AUROC, obtained by plotting the false positive rate [FP/(FP + TN)] on the x axis and the true positive rate (POD)

on the *y* axis, represents the ability of the model to separate the occurrence and nonoccurrence of RI. Finally, the BS is estimated as the mean squared difference between predicted probabilities and actual outcomes (Wilks 2011). Higher values of POD and AUROC, and lower values of FAR and BS indicate more skill.

To test model sensitivity, we use three different fractions of the data for the training set (55%, 60%, and 65%). In each case, we first use the various SHIPS-RII predictors as features to make predictions. Next, we include SSS along with those predictors to predict RI. All features are scaled between 0 and 1 before use in the model (Kaplan et al. 2010). If the inclusion of SSS increases the POD and AUROC and decreases the FAR and BS, then salinity is said to have improved the model performance. A Student's *t* test for difference of means is used to ascertain the statistical significance of the improvement in prediction. The Logistic model has been implemented using the "Scikit-learn" machine learning library in the Python programming language (http://scikit-learn.org). When implementing the model, we use the condition that the class weights are "balanced," which ensures that the weights are inversely proportional to the class frequencies. In other words, the model is penalized more when it fails to predict an RI event when compared to a non-RI event. Using this approach allows the model to be trained for handling relatively rare events such as RI.

We first use the SHIPS-RII predictors along with SSS from HYCOM for the 12-year period 2004–15. Next, to assess the value of satellite salinity for RI prediction, and to serve as an independent validation, we perform the same analysis using salinity from SMOS for the period 2010–17.

Results

We begin by examining the role of the ocean in TC intensification, focusing on RI. The domain of analysis is the region from 40° to 100°W and from 10° to 30°N. Nearly 90% of all locations where TCs underwent RI during the period 2002–18 are found in this domain, making it appropriate for our analysis. Figure 2a shows the anomalous mean prestorm SSTs, anomalous mean TC cold wakes, and anomalous mean enthalpy fluxes at the air–sea interface for various intensification rate thresholds. For instance, the anomalous mean SST corresponding to a threshold of 5 kt $(24\ h)^{-1}$ represents the difference between the mean SST for all 6-hourly track locations where the storm intensified by 5 kt or higher in 24 h and the SST averaged over all 6-hourly track locations. Similarly, the anomalous mean TC cold wake represents the mean SST cooling over all locations where the intensification rate exceeds a value minus the mean SST cooling over all locations. When computing the anomalous mean, we subsample data so that the initial intensity of the storm and its translation speed are statistically indifferent between the two sets. In other words, data are selected such that ranges for storm strength and forward moving speed are similar in the two datasets. Doing so allows us to remove the effects of the storm state and isolate the impacts of the ocean on TC intensification.

In general, the role of the ocean increases with the intensification rate of the TC (Fig. 2a), in line with past work (Lloyd and Vecchi 2011). While the anomalous mean enthalpy fluxes are not statistically significant for lower intensification rate thresholds, they are highly significant for larger intensification rate thresholds. For the 25 kt $(24\ h)^{-1}$ threshold and RI, the anomalous enthalpy fluxes are about 7.5 and 9.5 W m^{-2} higher, respectively. This indicates that for RI, the flux of heat from the ocean into the atmosphere becomes more important compared to weaker intensification rates. The enthalpy flux under the TC is critically dependent on the SST under the core of the storm (Cione and Uhlhorn 2003), which is a combination of the prestorm SST and the sea surface cooling induced by the TC. As expected, the anomalous mean prestorm SST increases with the TC's intensification rate. The anomalous mean SST is not significantly higher for all intensification rates greater than zero, but for RI the prestorm SST is about 0.3°C higher on average.

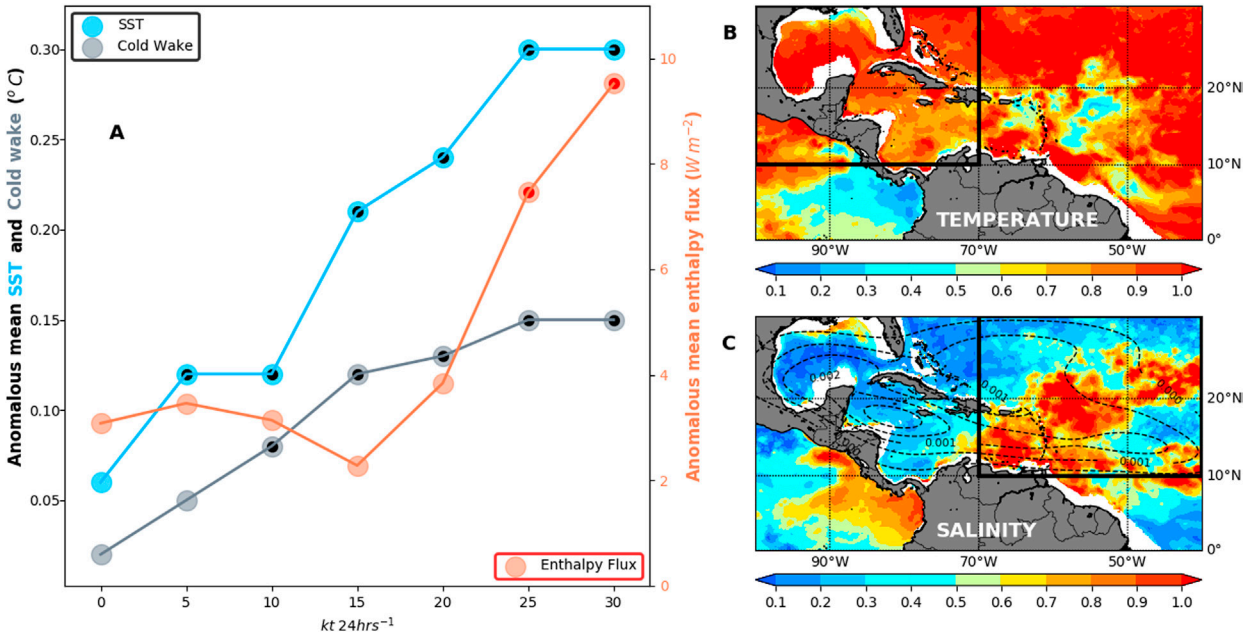

Fig. 2. (a) Anomalous mean prestorm SST (blue), cold wake (gray), and surface enthalpy flux (red) for Atlantic TCs as a function of intensification threshold. Anomalous mean represents the mean over all locations where the intensification rate exceeds a value minus the mean over all locations. While the total sample size is 2,674, sample sizes for various intensification thresholds are as follows: 1,641 [0 kt (24 h)$^{-1}$], 1,305 [5 kt (24 h)$^{-1}$], 988 [10 kt (24 h)$^{-1}$], 709 [15 kt (24 h)$^{-1}$], 493 [20 kt (24 h)$^{-1}$], 307 [25 kt (24 h)$^{-1}$], 205 [30 kt (24 h)$^{-1}$]. Concentric smaller dark circles indicate significance at the 95% level. (b) Coefficient of linear regression between density stratification and temperature stratification at a depth of 100 m. (c) As in (b), but for salinity stratification. Density, temperature, and salinity stratification have been normalized by subtracting their respective means and dividing by their standard deviations. Dashed contours in (c) show the locations of RI. The boxes approximately represent the subregions used for the analysis shown in Fig. 3. SST is from the satellite-based REMSS product, enthalpy flux is based on OAFlux, and ocean stratification (density, temperature, and salinity) is calculated from HYCOM.

Interestingly, the anomalous mean cold wakes become increasingly weaker with increasing intensification rates, as noted in previous studies (Lloyd and Vecchi 2011; Vincent et al. 2014). Note that a positive value for the anomalous mean wake does not indicate SST warming under a TC, but rather that the cold SST wake is weaker when compared to the mean wake. While the anomalous mean wake is not statistically significant for all intensification rates or the median intensification threshold [greater than or equal to 5 kt (24 h)$^{-1}$], for RI the anomalous mean cold wakes are significantly weaker by about 0.15°C. Thus, conditions in the ocean subsurface that cause a weakening of the cold TC wake likely play an important role in RI. These differences in cold wakes are likely due to those in upper-ocean stratification because we have subsampled our data to remove the effects of the storm state. Since both the vertical temperature and salinity structure jointly determine the ocean density stratification, it is important to evaluate which parameter dominates. To this end, we predict the upper-ocean density stratification using the normalized temperature and salinity stratification. Based on the regression coefficients (Figs. 2b,c), we can divide our domain broadly into two regions: 1) a western region where variability in the ocean thermal structure tends to dominate that in density (10°–30°N, 70°–100°W), and 2) an eastern region where salinity significantly modulates density stratification (10°–30°N, 40°–70°W). The western region includes the western Caribbean Sea and the Gulf of Mexico. In this region, warm upper-ocean features such as the Loop Current, and the eddies shed by it, induce variations in the ocean thermal structure. In the eastern region, freshwater outflow from the Amazon–Orinoco River system imposes significant constraints on the near-surface ocean density stratification.

To assess the impact of these spatial variations of temperature and salinity on TC RI, we compute TCHP, ocean stratification (density, temperature, and salinity), and SSS along TC tracks for each region. We consider two intensification rate threshold scenarios: 1) a median intensification threshold with intensification rates greater than or equal to 5 kt (24 h)$^{-1}$ and 2) RI. As before, for each threshold, we compute the anomalous mean TCHP, the anomalous mean ocean stratification (density, temperature, and salinity) and the anomalous mean SSS. For the western region (Fig. 3a), none of the parameters is statistically significant for the median intensification threshold, indicating the minimal role played by the ocean subsurface for weaker intensification rates. For RI, however, TCHP is highly significant and is larger by about 9.6 kJ cm^{-2} on average (Fig. 3b). This increase in significance for TCHP at higher intensification rates is consistent with previous studies (Mainelli et al. 2008; Kaplan et al. 2015). In regions with a deep thermocline and weak vertical temperature gradients, TC-induced mixing brings less cold water into the mixed layer, causing a reduction in the cold wake magnitude and favoring TC intensification. In the Gulf of Mexico for instance, several historical TCs have intensified rapidly over warm Loop Current eddies, such as Opal (1995) and Katrina (2005) (Shay et al. 2000; Mainelli et al. 2008; Lin et al. 2013). Consequently, TCHP has been shown to be a useful metric of the upper-ocean thermal structure for forecasting RI (Mainelli et al. 2008; Kaplan et al. 2010, 2015).

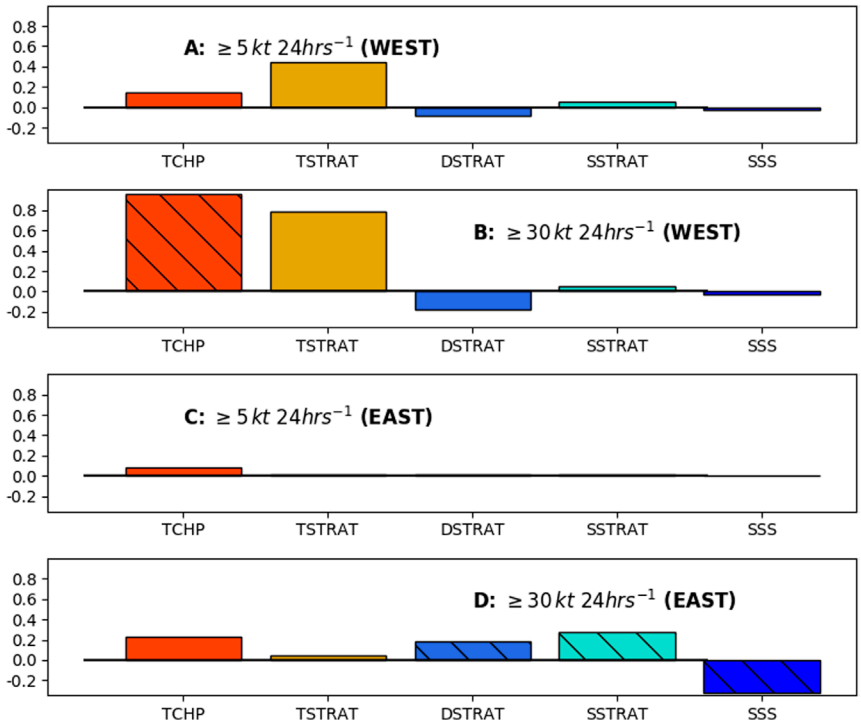

Fig. 3. Anomalous mean TCHP (10 kJ cm^{-2}), temperature stratification (TSTRAT; °C), density stratification (DSTRAT; kg m^{-3}), salinity stratification (SSTRAT; psu), and SSS (psu) in the (a),(b) western region and (c),(d) eastern region for cases where the 24-h intensity change is greater than or equal to (a),(c) 5 kt and (b),(d) RI. Anomalous mean represents the mean over all locations where the intensification rate exceeds a value minus the mean over all locations. The western region corresponds to 10°–30°N, 70°–100°W and the eastern region corresponds to 10°–30°N, 40°–70°W. For each parameter, when the mean of the subsampled data are statistically different from the total mean at the 95% level, it is indicated with hatching. TCHP, ocean stratification (DSTRAT, TSTRAT, and SSTRAT), and SSS are based on HYCOM.

In the eastern region, consistent with results from the western region, none of the oceanic parameters is statistically significant for the median intensification threshold (Fig. 3c). Even for RI, the anomalous mean TCHP and temperature stratification are not statistically significant (Fig. 3d). Note, however, that here we are only examining the subsurface—the anomalous mean SST is always significant for RI. The anomalous mean density and salinity stratification are highly significant for RI cases (Fig. 3d). On average, the density and salinity stratification are significantly higher by about 0.18 kg m^{-3} and 0.27 psu, respectively. In other words, the difference between the 100 m depth and surface values for density and salinity are larger. Since the anomalous mean temperature stratification is not statistically significant for RI, we can safely attribute the enhanced density stratification during RI events to that in salinity.

The mean intensity of weakly intensifying TCs in the western Atlantic is about 20 kt lower than the mean for RI. Hence, mixing is relatively shallow for weakly intensifying TCs. Thus,

even in the absence of strong stratification, the cooling induced at the surface is minimal and the ocean subsurface does not play an important role. On the other hand, at high intensification rates such as RI, the mixing extends considerably deeper. In this situation, without strong stratification that can limit mixing, substantial surface cooling tends to occur that can counteract the intensification of the storm. The freshwater plume of the Amazon–Orinoco River system enhances water column stability, reduces the mechanical mixing induced by TCs, and lowers the cold wake magnitude (Balaguru et al. 2012; Grodsky et al. 2012; Reul et al. 2014; Newinger and Toumi 2015; Androulidakis et al. 2016; Yan et al. 2017; Rudzin et al. 2019; Hlywiak and Nolan 2019). The anomalous mean SSS is significantly lower by 0.32 psu for RI (Fig. 3d), further supporting the idea that much of the salinity stratification encountered during RI is due to the low-salinity plume waters at the ocean surface. To test the robustness of our results, we performed similar analyses using the SODA 3.4.2 ocean reanalysis. Consistent relationships were obtained between ocean stratification and TC intensification, confirming the data independence of our main conclusions (Fig. ES2).

To further understand the effect of salinity on TC RI, we perform a suite of idealized numerical sensitivity experiments with the PWP one-dimensional ocean mixed layer model. The locations of the 20 different profiles of ocean temperature and salinity that were used to initialize the model are shown in Fig. 4a. All are in the region 10°–20°N, 50°–70°W, which is in close proximity to the Amazon–Orinoco plume. We use profiles during the months of

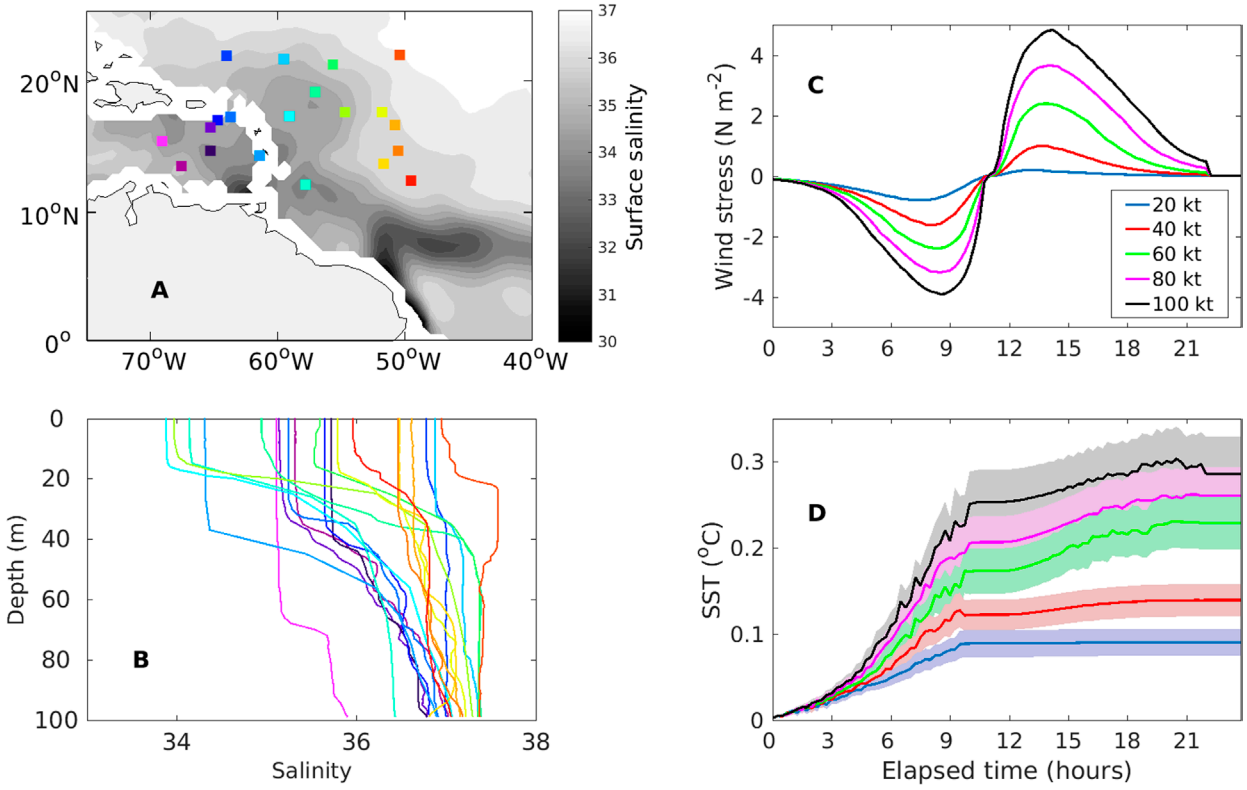

Fig. 4. (a) Shaded: September mean surface salinity from SMOS. Colored squares: locations of Argo temperature and salinity profiles used to initialize the one-dimensional PWP model. (b) Subsurface salinity from the floats at locations with matching colors shown in (a). (c) Zonal wind stress used to force the PWP model (meridional wind stress is always zero). For the control experiment, a maximum wind speed of 60 kt was used (green). Other colors show profiles for which the wind speed was either linearly increased (purple, black) or decreased (blue, red) to reach wind speed indicated in the legend at the second radius of maximum wind (see "Methods" section for details). (d) Results from the model experiments, showing difference in SST cooling between the simulations with full salinity and constant salinity (positive values indicate reduced cooling due to salinity stratification). The colors correspond to those of the wind profiles in (c) and shading indicates one standard error of the 20-member ensemble.

August–October, the climatological peak of the Atlantic TC season. An examination of the vertical structure of these profiles reveals the significance of salinity for ocean stratification in this region (Fig. 4b). In many cases, the mixed layer is confined to a depth of 20–30 m, below which salinity increases rapidly, by as much as 3 psu, over a depth of 50–60 m. We subject these profiles to TC winds representing various intensification rates, as shown in Fig. 4c. Although a three-dimensional ocean model is needed to reproduce the full impact of the TC on the ocean, the one-dimensional version of the model can reasonably capture the main effects when an ensemble approach is used (Hlywiak and Nolan 2019).

The time evolution of the difference in the ensemble mean SST between the experiments initialized with and without salinity stratification shows that the impact of salinity on SST increases with the intensification rate (Fig. 4d). For the cases with intensification relative to the 60 kt control simulation (purple and black curves in Fig. 4d), the inclusion of salinity reduces the TC-induced SST cooling by about 0.25°–0.3°C at hour 18. In contrast, for storms with less intensification (blue and red curves in Fig. 4d) the salinity-induced reduction in SST cooling is about 0.1°–0.15°C. The reduction in cooling caused by salinity stratification is about 0.1°C stronger for RI cases (black curve in Fig. 4d) compared to cases with no intensification (green curve in Fig. 4d), consistent with our earlier result (Fig. 2a). These results also indicate that the significance of salinity for RI is not due to collocated temperature features. If this were the case, the differences in SST cooling between the experiments with and without salinity would be close to zero.

Statistical RI prediction models have traditionally struggled more in the Atlantic than in some other basins (Kaplan et al. 2015). Since these models do not include a predictor based on salinity, and in light of the results in this study, we performed binary classification using logistic regression to evaluate the potential value of salinity for RI prediction. We conducted two sets of experiments. First, we used the various predictors included in SHIPS-RII to train the logistic model and predict the occurrence of RI. Next, we repeated this analysis with SSS included as an additional predictor. The main idea behind using SSS is to represent the effects of upper-ocean salinity stratification on TC-induced mixing. In the region influenced by the Amazon–Orinoco plume in the western tropical Atlantic, SSS primarily determines near-surface salinity stratification. The correlation between SSS and salinity stratification along TC tracks for the eastern region based on HYCOM data are about 0.9, suggesting that the former is a good indicator of the latter. But to what extent does SSS serve as a proxy for ocean density stratification?

To understand the connection between SSS and density stratification, we plot the correlation between the two for various minimum-salinity thresholds (Fig. ES3a). As the SSS threshold increases, the correlation between salinity and stratification decreases. This suggests that variations in SSS more accurately reflect those in density stratification for lower values of SSS and that SSS is a poor predictor of density stratification at higher values. The transition occurs near 36 psu, which approximately represents the boundary of the Amazon–Orinoco River plume (Pailler et al. 1999). Thus, considering only SSS values below about 36 psu could possibly improve the ability of salinity to separate RI from non-RI. To elucidate this point, we compute the means for salinity with and without RI while masking out salinity higher than a certain threshold each time. The plot of t values for statistical significance of the difference between means shows that the maximum t value is achieved near a threshold of 36 psu (Fig. ES3b). This statistical evidence further supports the idea of masking out higher salinity values. Physically, by doing this we allow salinity to vary primarily within the region influenced by the Amazon–Orinoco plume or other such locations with very fresh surface waters. We now use this masked SSS along with the other SHIPS-RII predictors in the logistic model. Results reveal that adding SSS to the logistic model significantly improves its skill (Table 1). The addition of SSS enhances the POD and AUROC, while lowering the FAR and the BS, reinforcing the value of salinity for RI prediction. Similar results are obtained when salinity

stratification is used instead of SSS, in agreement with the tight relationship between them in this region. Though we have demonstrated improvement in RI prediction using salinity from both reanalysis and satellite, the relative merits of each deserve further study.

Summary and discussion

The significance of the upper-ocean thermal structure for RI is well known. Consequently, related metrics such as TCHP have traditionally been used to represent the ocean in statistical RI prediction models. However, the role of salinity in RI is less clear. In this study, using a suite of observations and numerical model simulations, we have shown that salinity plays an important role in RI in the eastern Caribbean Sea and the western tropical Atlantic where the surface salinity and upper-ocean salinity stratification are heavily constrained by the freshwater plume of the Amazon–Orinoco River system. This is unlike the western Caribbean Sea and the Gulf of Mexico where temperature features dominate the ocean's impact on RI. Strong upper-ocean stratification is not particularly important for weaker intensification, where significant vertical mixing and sea surface cooling do not occur. On the other hand, stratification plays a pivotal role for RI because a substantial increase in mixing and SST cooling are more likely to occur when stratification is weaker. These results are supported by simulations with the PWP ocean mixed layer model, where we demonstrate that the influence of salinity on RI is independent of that of temperature, and that the relevance of salinity for a TC increases with its intensification rate. Finally, we tested the value of surface salinity, a reasonable proxy for upper-ocean salinity stratification in the Amazon–Orinoco plume region, for RI prediction. Results indicate that the use of SSS may significantly improve models' abilities to forecast RI.

Table 1. Estimating the significance of salinity for RI prediction in the North Atlantic. Results based on logistic model experiments. The first set of results (rows 1 and 2) is for the period 2004–15 using SSS from HYCOM ocean reanalysis. The second set of results (rows 3 and 4) is for the period 2010–17 using SSS from SMOS. The domain of analysis is the eastern region. In each set, the first row contains average skill scores for the model based on the SHIPS-RII predictors only. The second row contains the average scores for the model with SSS as an additional predictor. Values in bold indicate that the improvement in model obtained by the addition of salinity is statistically significant at the 95% level based on the respective scores.

	POD	FAR	AUROC	BS
SHIPS-RII	0.35	0.89	0.58	0.19
SHIPS-RII + SSS (HYCOM)	**0.44**	**0.85**	**0.62**	0.18
SHIPS-RII	0.53	0.77	0.70	0.18
SHIPS-RII + SSS (SMOS)	**0.58**	**0.74**	0.71	**0.17**

Efforts to incorporate salinity stratification into metrics of TC-induced SST cooling have been made in the past (Price 2009; Shay and Brewster 2010; Vincent et al. 2012; Balaguru et al. 2015), and the results from this study emphasize the need for continued progress along these lines. SST and sea level derived from satellites are being used for estimation of upper-ocean heat content and RI forecasting (Goni and Trinanes 2003; Shay and Brewster 2010). But satellite salinity observations, which have been available for nearly a decade, have not been used in weather forecasting to date. Near-continuous measurements of SSS are available from the SMOS satellite since May 2010 and from NASA's Soil Moisture Active Passive mission since April 2015 (Durack et al. 2016). Surface salinity measurements were also available from NASA's Aquarius mission between August 2011 and June 2015. Given the strong influence of the Amazon–Orinoco plume in the western Atlantic and eastern Caribbean, we advocate the use of satellite salinity in statistical RI prediction models, based on its prospects for improved forecasts (Table 1).

Though ocean reanalyses tend to do well in regions where they can assimilate a lot of in situ observations such as Argo profiles, satellite data can help in other regions where in situ measurements are relatively sparse (Tranchant et al. 2008; Lagerloef et al. 2010; Vernieres et al. 2014). For salinity, this is particularly true in regions near the coastline where surface salinity is heavily constrained by river runoff (Domingues et al. 2015;

Tranchant et al. 2008; Vernieres et al. 2014). It has been demonstrated that assimilating satellite salinity observations can significantly improve estimates of the upper-ocean state (Köhl et al. 2014; Toyoda et al. 2015; Vinogradova et al. 2019; Martin et al. 2019) and the climate of the Indo-Pacific region, including El Niño–Southern Oscillation (Hackert et al. 2014, 2019). Thus, besides their use in statistical RI models, satellite salinity could potentially improve ocean analyses used to initialize dynamical TC forecast models. Note that the results from the prediction model presented in this study are based on "perfect predictors" that are calculated from reanalyses in a "hindcast" mode. Though the results are very encouraging, further testing is required using real-time satellite and analysis data that are directly used in forecasts. We propose a study, along the lines of a Joint Hurricane Testbed, to further this cause and aid in the process of integrating salinity into operational RI forecasts.

Acknowledgments. K. B. and L. R. L. were supported by the Office of Science (BER), U.S. Department of Energy as part of the Regional and Global Modeling and Analysis (RGMA) Program. The Pacific Northwest National Laboratory is operated for DOE by Battelle Memorial Institute under Contract DE-AC05-76RL01830. G. F. was funded by base funds to NOAA/AOML's Physical Oceanography Division. K. B. and G. F. also acknowledge support from NOAA's Climate Program Office, Climate Monitoring Program (Award NA17OAR4310155). The various data used in this study are freely available for download from the sources provided in the "Methods" section.

Data availability statement: The sources for various data used in this study are provided in the "Data" section.

References

Androulidakis, Y., V. Kourafalou, G. Halliwell, M. Le Hénaff, H. Kang, M. Mehari, and R. Atlas, 2016: Hurricane interaction with the upper ocean in the Amazon-Orinoco plume region. *Ocean Dyn.*, **66**, 1559–1588, https://doi.org/10.1007/s10236-016-0997-0.

Avila, L. A., 2019: The 2018 Atlantic hurricane season: Another catastrophic year for the United States. *Weatherwise*, **72**, 14–21, https://doi.org/10.1080/00431672.2019.1612201.

Baker, D. J., M. Glackin, S. J. Roberts, R. W. Schmitt, E. S. Twigg, D. J. Vimont, and R. A. Weller, 2019: The challenge of sustaining ocean observations. *Front. Mar. Sci.*, **6**, 105, https://doi.org/10.3389/fmars.2019.00105.

Balaguru, K., P. Chang, R. Saravanan, L. R. Leung, Z. Xu, M. Li, and J.-S. Hsieh, 2012: Ocean barrier layers' effect on tropical cyclone intensification. *Proc. Natl. Acad. Sci. USA*, **109**, 14343–14347, https://doi.org/10.1073/pnas.1201364109.

——, G. R. Foltz, L. R. Leung, E. D. Asaro, K. A. Emanuel, H. Liu, and S. E. Zedler, 2015: Dynamic potential intensity: An improved representation of the ocean's impact on tropical cyclones. *Geophys. Res. Lett.*, **42**, 6739–6746, https://doi.org/10.1002/2015GL064822.

——, ——, and ——, 2018: Increasing magnitude of hurricane rapid intensification in the central and eastern tropical Atlantic. *Geophys. Res. Lett.*, **45**, 4238–4247, https://doi.org/10.1029/2018GL077597.

Bender, M. A., and I. Ginis, 2000: Real-case simulations of hurricane–ocean interaction using a high-resolution coupled model: Effects on hurricane intensity. *Mon. Wea. Rev.*, **128**, 917–946, https://doi.org/10.1175/1520-0493(2000)128<0917:RCSOHO>2.0.CO;2.

Boutin, J., J. Vergely, and S. Marchand, 2017: SMOS SSS L3 debias v2 maps generated by CATDS CEC LOCEAN, version 2.0. SEANOE, accessed June 2018, https://doi.org/10.17882/52804#54823.

Carton, J. A., G. A. Chepurin, and L. Chen, 2018: SODA3: A new ocean climate reanalysis. *J. Climate*, **31**, 6967–6983, https://doi.org/10.1175/JCLI-D-18-0149.1.

Chassignet, E. P., H. E. Hurlburt, O. M. Smedstad, G. R. Halliwell, P. J. Hogan, A. J. Wallcraft, R. Baraille, and R. Bleck, 2007: The HYCOM (Hybrid Coordinate Ocean Model) data assimilative system. *J. Mar. Syst.*, **65**, 60–83, https://doi.org/10.1016/j.jmarsys.2005.09.016.

Cione, J. J., and E. W. Uhlhorn, 2003: Sea surface temperature variability in hurricanes: Implications with respect to intensity change. *Mon. Wea. Rev.*, **131**, 1783–1796, https://doi.org/10.1175//2562.1.

DeMaria, M., 1987: Tropical cyclone track prediction with a barotropic spectral model. *Mon. Wea. Rev.*, **115**, 2346–2357, https://doi.org/10.1175/1520-0493(1987)115<2346:TCTPWA>2.0.CO;2.

——, M. Mainelli, L. K. Shay, J. A. Knaff, and J. Kaplan, 2005: Further improvements to the Statistical Hurricane Intensity Prediction Scheme (SHIPS). *Wea. Forecasting*, **20**, 531–543, https://doi.org/10.1175/WAF862.1.

Domingues, R., and Coauthors, 2015: Upper ocean response to Hurricane Gonzalo (2014): Salinity effects revealed by targeted and sustained underwater glider observations. *Geophys. Res. Lett.*, **42**, 7131–7138, https://doi.org/10.1002/2015GL065378.

Durack, P. J., T. Lee, N. T. Vinogradova, and D. Stammer, 2016: Keeping the lights on for global ocean salinity observation. *Nat. Climate Change*, **6**, 228–231, https://doi.org/10.1038/nclimate2946.

Emanuel, K. A., 1999: Thermodynamic control of hurricane intensity. *Nature*, **401**, 665–669, https://doi.org/10.1038/44326.

——, 2017: Will global warming make hurricane forecasting more difficult? *Bull. Amer. Meteor. Soc.*, **98**, 495–501, https://doi.org/10.1175/BAMS-D-16-0134.1.

Gall, R., J. Franklin, F. Marks, E. N. Rappaport, and F. Toepfer, 2013: The Hurricane Forecast Improvement Project. *Bull. Amer. Meteor. Soc.*, **94**, 329–343, https://doi.org/10.1175/BAMS-D-12-00071.1.

Goni, G. J., and J. A. Trinanes, 2003: Ocean thermal structure monitoring could aid in the intensity forecast of tropical cyclones. *Eos, Trans. Amer. Geophys. Union*, **84**, 573–578, https://doi.org/10.1029/2003EO510001.

Grodsky, S. A., and Coauthors, 2012: Haline hurricane wake in the Amazon/Orinoco plume: AQUARIUS/SACD and SMOS observations. *Geophys. Res. Lett.*, **39**, L20603, https://doi.org/10.1029/2012GL053335.

Hackert, E., A. J. Busalacchi, and J. Ballabrera-Poy, 2014: Impact of Aquarius sea surface salinity observations on coupled forecasts for the tropical Indo-Pacific Ocean. *J. Geophys. Res. Oceans*, **119**, 4045–4067, https://doi.org/10.1002/2013JC009697.

——, R. M. Kovach, A. J. Busalacchi, and J. Ballabrera-Poy, 2019: Impact of Aquarius and SMAP satellite sea surface salinity observations on coupled el niño/southern oscillation forecasts. *J. Geophys. Res. Oceans*, **124**, 4546–4556, https://doi.org/10.1029/2019JC015130.

Hlywiak, J., and D. S. Nolan, 2019: The influence of oceanic barrier layers on tropical cyclone intensity as determined through idealized, coupled numerical simulations. *J. Phys. Oceanogr.*, **49**, 1723–1745, https://doi.org/10.1175/JPO-D-18-0267.1.

Kaplan, J., and M. DeMaria, 2003: Large-scale characteristics of rapidly intensifying tropical cyclones in the North Atlantic basin. *Wea. Forecasting*, **18**, 1093–1108, https://doi.org/10.1175/1520-0434(2003)018<1093:LCORIT>2.0.CO;2.

——, M. DeMaria, and J. A. Knaff, 2010: A revised tropical cyclone rapid intensification index for the Atlantic and eastern North Pacific basins. *Wea. Forecasting*, **25**, 220–241, https://doi.org/10.1175/2009WAF2222280.1.

——, and Coauthors, 2015: Evaluating environmental impacts on tropical cyclone rapid intensification predictability utilizing statistical models. *Wea. Forecasting*, **30**, 1374–1396, https://doi.org/10.1175/WAF-D-15-0032.1.

Klotzbach, P. J., C. J. Schreck III, J. M. Collins, M. M. Bell, E. S. Blake, and D. Roache, 2018: The extremely active 2017 North Atlantic hurricane season. *Mon. Wea. Rev.*, **146**, 3425–3443, https://doi.org/10.1175/MWR-D-18-0078.1.

Köhl, A., M. Sena Martins, and D. Stammer, 2014: Impact of assimilating surface salinity from SMOS on ocean circulation estimates. *J. Geophys. Res. Oceans*, **119**, 5449–5464, https://doi.org/10.1002/2014JC010040.

Kowch, R., and K. Emanuel, 2015: Are special processes at work in the rapid intensification of tropical cyclones? *Mon. Wea. Rev.*, **143**, 878–882, https://doi.org/10.1175/MWR-D-14-00360.1.

Lagerloef, G., and Coauthors, 2010: Resolving the global surface salinity field and variations by blending satellite and in situ observations. *Proceedings of OceanObs'09: Sustained Ocean Observations and Information for Society (Vol. 2)*, J. Hall, D. E. Harrison, and D. Stammer, Eds., ESA Publication WPP-306, European Space Agency, https://doi.org/10.5270/OceanObs09.cwp.51.

Landsea, C. W., and J. L. Franklin, 2013: Atlantic hurricane database uncertainty and presentation of a new database format. *Mon. Wea. Rev.*, **141**, 3576–3592, https://doi.org/10.1175/MWR-D-12-00254.1.

Lee, C.-Y., M. K. Tippett, A. H. Sobel, and S. J. Camargo, 2016: Rapid intensification and the bimodal distribution of tropical cyclone intensity. *Nat. Commun.*, **7**, 10625, https://doi.org/10.1038/ncomms10625.

Lin, I.-I., G. J. Goni, J. A. Knaff, C. Forbes, and M. Ali, 2013: Ocean heat content for tropical cyclone intensity forecasting and its impact on storm surge. *Nat. Hazards*, **66**, 1481–1500, https://doi.org/10.1007/s11069-012-0214-5.

Lloyd, I. D., and G. A. Vecchi, 2011: Observational evidence for oceanic controls on hurricane intensity. *J. Climate*, **24**, 1138–1153, https://doi.org/10.1175/2010JCLI3763.1.

Mainelli, M., M. DeMaria, L. K. Shay, and G. Goni, 2008: Application of oceanic heat content estimation to operational forecasting of recent Atlantic category 5 hurricanes. *Wea. Forecasting*, **23**, 3–16, https://doi.org/10.1175/2007WAF2006111.1.

Martin, M. J., R. R. King, J. While, and A. B. Aguiar, 2019: Assimilating satellite sea-surface salinity data from SMOS, Aquarius and SMAP into a global ocean forecasting system. *Quart. J. Roy. Meteor. Soc.*, **145**, 705–726, https://doi.org/10.1002/qj.3461.

Newinger, C., and R. Toumi, 2015: Potential impact of the colored Amazon and Orinoco plume on tropical cyclone intensity. *J. Geophys. Res. Oceans*, **120**, 1296–1317, https://doi.org/10.1002/2014JC010533.

Pailler, K., B. Bourlès, and Y. Gouriou, 1999: The barrier layer in the western tropical Atlantic Ocean. *Geophys. Res. Lett.*, **26**, 2069–2072, https://doi.org/10.1029/1999GL900492.

Price, J. F., 1981: Upper ocean response to a hurricane. *J. Phys. Oceanogr.*, **11**, 153–175, https://doi.org/10.1175/1520-0485(1981)011<0153:UORTAH>2.0.CO;2.

——, 2009: Metrics of hurricane-ocean interaction: Vertically-integrated or vertically-averaged ocean temperature? *Ocean Sci.*, **5**, 351–368, https://doi.org/10.5194/os-5-351-2009.

——, R. A. Weller, and R. Pinkel, 1986: Diurnal cycling: Observations and models of the upper ocean response to diurnal heating, cooling, and wind mixing. *J. Geophys. Res.*, **91**, 8411–8427, https://doi.org/10.1029/JC091iC07p08411.

Rahmstorf, S., 2017: Rising hazard of storm-surge flooding. *Proc. Natl. Acad. Sci. USA*, **114**, 11 806–11 808, https://doi.org/10.1073/PNAS.1715895114.

Reul, N., Y. Quilfen, B. Chapron, S. Fournier, V. Kudryavtsev, and R. Sabia, 2014: Multisensor observations of the Amazon-Orinoco River plume interactions with hurricanes. *J. Geophys. Res. Oceans*, **119**, 8271–8295, https://doi.org/10.1002/2014JC010107.

Rozoff, C. M., and J. P. Kossin, 2011: New probabilistic forecast models for the prediction of tropical cyclone rapid intensification. *Wea. Forecasting*, **26**, 677–689, https://doi.org/10.1175/WAF-D-10-05059.1.

Rudzin, J. E., L. K. Shay, and B. Jaimes de la Cruz, 2019: The impact of the Amazon–Orinoco River plume on enthalpy flux and air–sea interaction within Caribbean Sea tropical cyclones. *Mon. Wea. Rev.*, **147**, 931–950, https://doi.org/10.1175/MWR-D-18-0295.1.

Sena Martins, M., N. Serra, and D. Stammer, 2015: Spatial and temporal scales of sea surface salinity variability in the Atlantic Ocean. *J. Geophys. Res. Oceans*, **120**, 4306–4323, https://doi.org/10.1002/2014JC010649.

Shay, L. K., and J. K. Brewster, 2010: Oceanic heat content variability in the eastern Pacific Ocean for hurricane intensity forecasting. *Mon. Wea. Rev.*, **138**, 2110–2131, https://doi.org/10.1175/2010MWR3189.1.

——, G. J. Goni, and P. G. Black, 2000: Effects of a warm oceanic feature on Hurricane Opal. *Mon. Wea. Rev.*, **128**, 1366–1383, https://doi.org/10.1175/1520-0493(2000)128<1366:EOAWOF>2.0.CO;2.

Stewart, S. R., 2017: Tropical cyclone report: Hurricane Matthew (AL142016) 28 September–9 October 2016. National Hurricane Center, www.nhc.noaa.gov/data/tcr/index.php?season=2016&basin=atl.

Toyoda, T., and Coauthors, 2015: Improvements to a global ocean data assimilation system through the incorporation of Aquarius surface salinity data. *Quart. J. Roy. Meteor. Soc.*, **141**, 2750–2759, https://doi.org/10.1002/qj.2561.

Tranchant, B., C.-E. Testut, L. Renault, N. Ferry, F. Birol, and P. Brasseur, 2008: Expected impact of the future SMOS and Aquarius ocean surface salinity missions in the Mercator ocean operational systems: New perspectives to monitor ocean circulation. *Remote Sens. Environ.*, **112**, 1476–1487, https://doi.org/10.1016/j.rse.2007.06.023.

Vernieres, G., R. Kovach, C. Keppenne, S. Akella, L. Brucker, and E. Dinnat, 2014: The impact of the assimilation of Aquarius sea surface salinity data in the GEOS ocean data assimilation system. *J. Geophys. Res. Oceans*, **119**, 6974–6987, https://doi.org/10.1002/2014JC010006.

Vincent, E. M., M. Lengaigne, J. Vialard, G. Madec, N. C. Jourdain, and S. Masson, 2012: Assessing the oceanic control on the amplitude of sea surface cooling induced by tropical cyclones. *J. Geophys. Res.*, **117**, C05023, https://doi.org/10.1029/2011JC007705.

——, K. A. Emanuel, M. Lengaigne, J. Vialard, and G. Madec, 2014: Influence of upper ocean stratification interannual variability on tropical cyclones. *J. Adv. Model. Earth Syst.*, **6**, 680–699, https://doi.org/10.1002/2014MS000327.

Vinogradova, N., and Coauthors, 2019: Satellite salinity observing system: Recent discoveries and the way forward. *Front. Mar. Sci.*, **6**, 243, https://doi.org/10.3389/fmars.2019.00243.

Wilks, D. S., 2011: *Statistical Methods in the Atmospheric Sciences*. 3rd ed. International Geophysics Series, Vol. 100, Academic Press, 704 pp.

Yan, Y., L. Li, and C. Wang, 2017: The effects of oceanic barrier layer on the upper ocean response to tropical cyclones. *J. Geophys. Res. Oceans*, **122**, 4829–4844, https://doi.org/10.1002/2017JC012694.

Yu, L., X. Jin, and R. Weller, 2008: Multidecade global flux datasets from the Objectively Analyzed Air-Sea Fluxes (OAFlux) Project: Latent and sensible heat fluxes, ocean evaporation, and related surface meteorological variables. Woods Hole Oceanographic Institution OAFlux Project Tech. Rep. OA-2008-01, 64 pp.